POLITECNICO DI TORINO
Repository ISTITUZIONALE

Osteoporosis-related variations of trabecular bone properties of proximal human humeral heads at different scale lengths

Original
Osteoporosis-related variations of trabecular bone properties of proximal human humeral heads at different scale lengths / Molino, G., Dalpozzi, A., Ciapetti, G., Lorusso, M., Novara, C., Cavallo, M., Baldini, N., Giorgis, F., Fiorilli, S.L., VITALE BROVARONE, C.. - In: JOURNAL OF THE MECHANICAL BEHAVIOR OF BIOMEDICAL MATERIALS. - ISSN 1751-6161. - ELETTRONICO. - 100:(2019). [10.1016/j.jmbbm.2019.103373]

Availability:
This version is available at: 11583/2753037 since: 2020-04-14T14:50:19Z

Publisher:
Elsevier

Published
DOI:10.1016/j.jmbbm.2019.103373

Terms of use:

This article is made available under terms and conditions as specified in the corresponding bibliographic description in the repository

Publisher copyright

(Article begins on next page)

29 November 2026

Journal of the Mechanical Behavior of Biomedical Materials 100 (2019) 103373

Contents lists available at ScienceDirect

Journal of the Mechanical Behavior of Biomedical Materials

journal homepage: www.elsevier.com/locate/jmbbm

Osteoporosis-related variations of trabecular bone properties of proximal human humeral heads at different scale lengths

Molino Giulia[a], Dalpozzi Alessio[a], Ciapetti Gabriela[b], Lorusso Massimo[c], Novara Chiara[a], Cavallo Marco[d], Baldini Nicola[e], Giorgis Fabrizio[a], Fiorilli Sonia[a], Vitale-Brovarone Chiara[a,*]

[a] Politecnico di Torino, Department of Applied Science and Technology, Corso Duca degli Abruzzi 24, 10129, Torino, Italy
[b] Laboratory for Orthopaedic Pathophysiology and Regenerative Medicine, IRCCS Istituto Ortopedico Rizzoli, Bologna, Italy
[c] Center for Sustainable Future Technologies@Polito, Istituto Italiano di Tecnologia, Via Livorno 60, 10145, Torino, Italy
[d] Shoulder and Elbow Surgery Unit, IRCCS Istituto Ortopedico Rizzoli, Bologna, Italy
[e] Laboratory for Orthopaedic Pathophysiology and Regenerative Medicine, IRCCS Istituto Ortopedico Rizzoli, & Department of Biomedical and Neuromotor Sciences, University of Bologna, Italy

ARTICLE INFO

Keywords:
Osteoporosis
Humeral head
Micro-CT
Compression test
Nanoindentation
Raman spectroscopy

ABSTRACT

Osteoporosis (OP) is a skeletal disorder responsible for the weakening of the bone structure and, consequently, for an increased fracture risk in the elderly population. In the past, bone mineral density (BMD) variation was considered the best OP indicator, but recently the focus has shifted toward the variation of microstructural bone parameters. This work is based on the characterisation of 8-mm cylindrical biopsies harvested from proximal humeral heads belonging to healthy and osteoporotic patients, in order to assess the OP-related variations of bone properties at different scale lengths. In particular, bone biopsies underwent micro-computed tomography analysis to study the most relevant features of bone architecture and extrapolate the tissue mineral density (TMD) value of bone trabeculae. Compression tests and nanoindentations were performed to investigate the macro- and micromechanical properties of bone biopsies, respectively. In addition, XRD analyses were performed to obtain the mean hydroxyapatite (HA) crystallite size, while Raman spectroscopy investigated the collagen secondary structure. Thermogravimetric analysis was performed to evaluate the ratio between organic and inorganic phases.

From the obtained results, OP samples showed a more anisotropic and less interconnected structure responsible for reduced compression strength. From this, it can be supposed that OP caused an alteration of bone structure that led to inferior macroscopic mechanical properties. Furthermore, OP samples possessed higher TMD and bigger HA crystals that are correlated to an increase of the hardness value obtained by means of nanoindentation. This less controlled HA crystal growth is probably due to an alteration of the organic matrix structure, as revealed by the increase of the random coil contribution in the Raman spectra of the OP bone. This higher crystal content led to an increase in trabecular density and hardness. In conclusion, the obtained data showed that OP affects bone properties at different scale lengths causing an alteration of its morphological, structural and mechanical features.

1. Introduction

Osteoporosis (OP) is a worldwide skeletal disorder caused by a disproportion between osteoclast and osteoblast activity leading to bone resorption predominance. This imbalanced mechanism leads to the reduction of bone mass and to the decrease of its quality, with a consequent increase of fracture risk (Osterhoff et al., 2016). Since OP affects predominantly the elderly population, as well as a high proportion of post-menopausal women, osteoporotic fractures can lead to several consequences such as decreased quality of life, loss of independent living, decline in health status and even death (Glowacki and Vokes, 2016). For this reason, osteoporotic patients should be adequately diagnosed and treated for fracture prevention.

Conventionally OP is diagnosed on the basis of dual-energy X-ray absorptiometry (DXA) measurement at the spine or the hip and it is defined as a value of bone mineral density (BMD) that lies more than 2.5 standard deviations below the mean BMD registered for healthy young adults (Dimai, 2017).

* Corresponding author.
E-mail address: chiara.vitale@polito.it (V.-B. Chiara).

https://doi.org/10.1016/j.jmbbm.2019.103373
Received 29 January 2019; Received in revised form 1 April 2019; Accepted 25 July 2019
Available online 26 July 2019
1751-6161/ © 2019 The Authors. Published by Elsevier Ltd. This is an open access article under the CC BY-NC-ND license (http://creativecommons.org/licenses/BY-NC-ND/4.0/).

Table 1
Proximal humeral head sample classification.

Sample groups	Number of samples	Age range (years)	Mean Age (years)	Males number	Females Number
Healthy (H)	7	50–70	62.9	2	5
Healthy Old (HO)	3	70–90	77.3	3	–
Osteoporotic (OP)	2	50–90	78.5	–	2
Osteopenic (OPen)	1	50–90	64	–	1

However, the measure of BMD through non-invasive methods as a surrogate marker of bone strength is considered even less reliable. Indeed, a large overlap of BMD values has been found between healthy people and those who have experienced OP bone fractures (Genant et al., 2008; Ozan et al., 2017). The structural arrangement of bone at macroscopic and microscopic levels, together with mineralisation and collagen matrix properties, are now considered better indicators of bone quality, useful to predict the OP-associated fracture risk (Gourion-Arsiquaud et al., 2009; Lloyd et al., 2015).

For this reason, many research studies have focused on the assessment of bone structural variations due to ageing and OP at the most common osteoporotic fracture sites (Chen, 2014; Rho et al., 1995; Stauber and Müller, 2006), femoral head being the most investigated one. Indeed, several works have demonstrated the strong correlation between bone volume fraction and the mechanical properties of the femoral head: inferior mechanical performances have been reported for fractured bones due to their reduced bone volume fraction (Berot et al., 2012; Ciarallo et al., 2006; Ciarelli et al., 2000).

Some research groups have also compared the structural and mechanical properties of osteoporotic and osteoarthritic femoral heads, evidencing again an inferior compressive strength for OP samples correlated to their reduced bone volume fraction (Li and Aspden, 1997; Nikodem, 2012; Vale et al., 2013; Zhang et al., 2010).

In the last decade, the assessment of the organic matrix modifications with age and OP, and the investigation of their influence on bone behaviour has gained increasing attention. Raman and Fourier transform infrared (FTIR) spectroscopies are usually employed in bone characterisation since these techniques can provide relevant information on the composition and the arrangement of the organic matrix (Morris and Mandair, 2011). In particular, the analysis of the amide I bands obtained through Raman spectroscopy can reveal the collagen secondary structure and consequently it can provide a measure of its quality. As recently reported, Raman analyses performed on OP bones show an alteration of collagen conformation and organisation (Toledano et al., 2018).

Even though proximal humerus is the third most common site for osteoporotic fractures after wrist and hip (Launonen et al., 2015), there is a lack of studies on the assessment of OP influence on its structural features. Most articles concerning this anatomical region focus on the assessment of bone mineral density (BMD) variation across the entire humeral head structure with the aim of finding the most appropriate region for prosthesis fixation (Alidousti et al., 2017; Saitoh et al., 1994; Tingart et al., 2003). Indeed, osteoporotic fracture treatment is often associated with a much higher failure rate of implant fixation compared with healthy patients due to the diminished healing capacity of OP bone (Sterling and Guelcher, 2014). However, as already mentioned, BMD is not the only factor influencing the bone quality, as a significant role is also played by bone micro-architectural characteristics (Osterhoff et al., 2016). For this reason, many studies have focused on the assessment of humeral structural features through morphometric analyses, such as histomorphometry (Barvencik et al., 2010; Hepp et al., 2003; Sprecher et al., 2015) and peripheral quantitative computed tomography (pQCT) (Mantila Roosa et al., 2012). These studies have aimed to correlate the structural properties of bone to its mechanical strength or to evaluate the possible age and gender-related variations.

In this work, the morphological characterisation of healthy and osteoporotic proximal humeral heads through high-resolution micro-computed tomography (micro-CT) was performed. There were two main advantages to this technique: it avoided the staining of samples, required by histomorphometry, and it worked with higher resolutions compared to other CT techniques, such as pQCT (Genant et al., 2008). Furthermore, mechanical tests at macroscopic and microscopic levels were executed through compression and nanoindentation respectively, and their correlations with morphological parameters were investigated. Bone properties at the sub-microscopic level were investigated through X-ray diffraction and Raman spectroscopy in order to evaluate the possible OP-related variations of HA crystal size and collagen matrix organisation, respectively.

Since in the literature there is a lack of studies concerning the analysis of osteoporosis-related changes of humeral head properties at different scale lengths, this work introduces significant results in this under-investigated anatomical site.

2. Materials and methods

2.1. Materials

Thirteen proximal human humeral heads were collected from male and female patients undergoing shoulder arthroplasty at the Istituto Ortopedico Rizzoli (Bologna, Italy). The study was approved by the IOR Ethical Committee and donors agreed to be part of the study by signing a written informed consensus. The samples were subdivided into four main groups: osteoporotic (OP), osteopenic (OPen), healthy (H) and healthy old (HO). The osteoporotic and osteopenic classification was based on dual-energy X-ray absorptiometry diagnosis of the patients. Group classification, age range and number of samples belonging to each group are reported in Table 1. One of the osteoporotic samples was excluded from the study because the patient was under drug treatment that altered the original bone structure. After surgical intervention, bone samples were cleaned from soft tissues and were fixed in 10% neutral buffered formalin solution (NBF) for a period between 7 and 14 days. Then the samples were washed in phosphate buffered solution (PBS) to remove NBF residues and were soaked in 70 vol% ethanol solution at 4 °C for long-term storage.

From each humeral head, several biopsies were harvested using a dental drill (X2i, Mariotti) with an 8-mm diameter head (Komet). The resulting samples had a mean diameter of 7.66 mm and a height comprised between 10 and 25 mm according to their anatomical site. Due to the approximatively semi-spherical shape of the humeral heads, the highest biopsies were obtained from the central region, while the smallest from the lateral and inferior regions.

2.2. Micro-CT analyses

Micro-CT analyses were carried out on biopsies through a high-resolution device, SkyScan 1272 (Bruker). Prior to analysis, biopsies were rehydrated overnight in PBS, then they were wrapped with tissue paper, inserted in a plastic tube and wetted with PBS. This procedure avoided the sample drying during scanning and reproduced physiologic-like conditions. Biopsies were scanned with the following parameters: resolution 3 μm, voltage 90 kV, current 110 mA, combined aluminium and copper filter (thickness 0.5 and 0.038 mm, respectively) and

rotation step 0.1°. The acquired images were reconstructed through a specific software (N-Recon, Bruker) and a cylindrical volume of interest (VOI) of 5 mm in diameter and 5 mm in height was selected in each biopsy, in order to exclude the superficial bone fragments generated during the harvesting procedure. After an operation of binarisation, indispensable to differentiate univocally bone structure from less dense materials, morphometric analyses were performed on the selected VOI through a specific software (CTAn, Bruker). The structural parameters obtained by morphometric analyses that were considered are the following: *Total Pore Percentage* (Po.Tot, %); *Trabecular Thickness* (Tb.Th, μm); *Trabecular Separation* (Tb.Sp, μm); *Degree of Anisotropy* (DA, none) where 0 corresponds to a high isotropic structure while 1 to an anisotropic one; *Trabecular Bone Pattern Factor* (Tb.Pf, mm^{-1}) that is an inverse index of connectivity. Furthermore, by comparing the X-ray absorption level of biopsies with two reference phantoms, having a known hydroxyapatite concentration and subjected to the same scanning and reconstruction processes, the *Tissue Mineral Density* (TMD) was calculated.

2.3. Compression tests

After micro-CT analyses, biopsies were cut with a goldsmith saw, orthogonally to the longitudinal axis, in order to remove the cortical region and to get regular cylindrical samples for uniaxial compression tests. The mean sample height after the saw cutting was 7.38 mm, thus obtaining an aspect ratio (length/diameter) close to one. Prior to the test, bone cylinders were rehydrated overnight in PBS and their height and diameter were measured. The compression tests were performed through the CRITERION C43.504 system (MTS) with a load cell of 5 kN and a cross-head speed of 1 mm/min. The tests were ended when a compression value of 4 mm was reached.

After an operation of non-linear curve fitting, inspiring to the procedure adopted by Aleixo et al. (2012), the value of compressive stress recorded at 30% of strain was considered as failure stress (σ_f) and was utilised for the successive correlation analyses (see section 2.8).

2.4. X-ray diffraction measurements

In order to obtain a powder, samples that underwent compression tests were successively dehydrated by a sequential soaking in ethanol solution with increasing concentrations (70%-80%-95%–100%). Then, they were defatted in acetone for 2 h, dried in oven at 100 °C for 24 h and finally hand crushed in an agate mortar. X-ray diffraction (XRD) measurements were performed using CuKα radiation at 40 kV and 40 mA (X'Pert PRO, PANalytical) from 10 to 80° 2θ. On the acquired spectrum, the Scherrer equation was applied for the calculation of the hydroxyapatite (HA) crystallite dimension, after an appropriate peak analysis procedure. For this calculation, the peak placed at 25.8° 2θ was chosen since it corresponds to the long axis (c-axis) of HA and does not present overlaps with other peaks (Fathi et al., 2008).

2.5. Raman spectroscopy

Raman spectroscopy measurements were performed on healthy and OP biopsies in order to analyse the bone matrix organisation. Prior to analyses, biopsies were rehydrated overnight in PBS and were subjected to three washing cycles in PBS, to remove bone marrow, and to one cycle in distilled water, to wash away possible PBS residues.

After this procedure, biopsies were subjected to Raman analysis through a micro-Raman spectrometer (InVia, Renishaw). In particular, a laser source with a wavelength of 785 nm was focused on the sample through a 5× objective at a power of 125 mW, collecting the signal in a backscattering configuration. The acquisition time was 100 s. The investigated Raman shift range was from 720 to 1810 cm^{-1}. Measurements were performed on five different trabeculae for each bone group and successively the average spectrum was calculated.

The peak analysis of the Raman spectra was focused on amide I region, studying the OP-related variations of three principal peaks recognised in the literature as indicators of collagen conformation: random coil (1686 cm^{-1}), α-helix (1666 cm^{-1}) and β-sheet (1636 cm^{-1}) (Pezzotti et al., 2017). The deconvolution of the amide I band was performed by OriginPro (2016) fitting tool.

Despite several washing cycles, bone marrow contribution was significant in the Raman pattern of bone samples. A band due to lipid residuals was indeed observed in the amide I region (at 1660 cm^{-1}), potentially leading to a not reliable interpretation of the collagen peaks. In order to quantify this lipid contribution, Raman spectra of bone marrow as such were acquired. Since the lipid peak placed at 1745 cm^{-1} does not present any overlapping in the bone spectrum, it was taken as a reference to estimate the lipid contribution to the amide I band. Thus, the ratio between 1660 and 1745 cm^{-1} lipid band areas of the bone marrow sample was calculated. Successively, this ratio was used to derive the area of the 1660 cm^{-1} lipid peak of the bone sample, after measuring the area of the 1745 cm^{-1} one. By imposing the so-calculated lipid peak area in the deconvolution, a reliable identification of collagen peaks in the amide I region was obtained.

2.6. Nanoindentation tests

Nanoindentation tests were performed on healthy and OP biopsies in order to assess the mechanical properties of bone at the microscale. Sample preparation procedure consisted in a dehydration and defatting phase similar to that performed for XRD measurements, followed by the embedding in epoxy resin (EpoFix Resin, Struers). Successively, the embedded samples were polished by a rotational polishing machine (Mecatech 234, Presi) first with silicon carbide abrasive papers with decreasing particle size (320-800-1200-2000-4000 grit) and then with 3 μm diamond paste.

Nanoindentation tests were performed by Hysitron TI 950 Triboindenter (Bruker), with a 3-side diamond pyramid tip (Berkovich tip), characterised by an included angle of 142.3° and by an angle with the normal to face equal to 65.35°. The tests were conducted in load-controlled conditions, reaching the maximum load of 5 mN. The loading and the unloading rates were set to 100 μN/s while the maximum load was held for 20 s. No drift compensation for the viscous effect of bone tissue was applied since it is reported in the literature to have a very low influence (≈1%) on data (Zysset et al., 1999).

Through the application of the Oliver-Pharr method (Oliver and Pharr, 1992), the reduced modulus (E_r) and the hardness value (H_c) were extrapolated from the slope of the unloading curve and from the indentation area, respectively. The reduced modulus does not take into account the elasticity of the diamond tip, but since its stiffness is very high compared to bone (E = 1140 GPa and $\nu = 0.07$), its influence is negligible (Fratzl-Zelman et al., 2009).

For each bone sample, three different trabeculae were selected and a nanoindentation grid was drawn in order to evaluate the E_r and H_c variations along the entire trabeculae thickness. The distance between each nanoindentation was set equal to 7.5 μm.

2.7. Thermogravimetric analyses

Thermogravimetric analyses (TGA) were performed on post-compression samples, one for each proximal humeral head, that were dehydrated and defatted and hand crushed similarly to XRD preparation method in order to obtain a powder. Approximately 10 mg of trabecular bone underwent TGA analyses (Q500, TA Instruments) in air atmosphere from room temperature to 800 °C with a heating rate of 10 °C/min.

2.8. Statistical methods

Statistical differences between groups (H/HO/OP/OPen) were

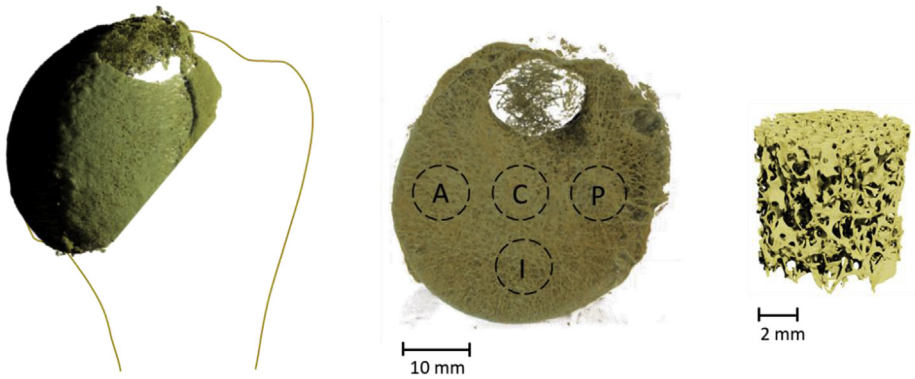


Fig. 1. Micro-CT reconstruction of a left proximal humeral head (left), schematic representation of biopsies harvesting area (middle) and micro-CT reconstruction of a representative 8-mm biopsy (right).

investigated through one-way ANOVA using Tukey's pairwise post-hoc test and imposing an interval of confidence of 95% for each characterisation method. Statistical significance was represented as $^{*}p < 0.05$. Additionally, site variations of micro-CT morphometric parameters were analysed through the same statistical method to highlight eventual significant trends between anatomical regions (Central/Anterior/Posterior/Inferior) of proximal humeral heads.

To assess correlations among morphometric, structural and mechanical parameters, Pearson's coefficients were calculated, imposing an interval of confidence of 95%.

3. Results and discussion

3.1. Micro-CT analyses

Biopsies harvested from human humeral heads were classified as follow: anterior (A), central (C), posterior (P) and inferior (I). A schematic representation of the biopsy harvesting area of a left humeral head and the micro-CT reconstruction of a representative biopsy are visible in Fig. 1.

Morphometric analyses performed on biopsies through micro-CT showed that the most significant differences between groups concerned DA and TMD parameters (Fig. 2). In particular, OP and OPen samples showed increased DA compared to H and HO samples, indicating the presence of a more anisotropic structure for unhealthy bone samples.

Furthermore, TMD was significantly higher for OP samples compared to all the other groups. Since TMD is defined as the density of calcified bone tissue, excluding soft tissue and porosity contributions, it is possible to deduct that OP sample is made of denser trabeculae. This increase in density can reflect a higher amount of inorganic phase.

Concerning the other morphometric parameters, no statistical differences were found, with the exception of Po.To and Tb.Th variations between OP and OPen samples. Indeed, OPen biopsies showed a higher mean Tb.Th that justified the reduction of their mean porosity value, despite a high variability among the different anatomical regions. The lowest Tb.Th values were recorded for the OP biopsies, confirming that the increased bone resorption rate due to osteoporosis causes the thinning of the trabecular structure.

Even if not statistically significant, OP sample showed a higher Tb.Pf value compared to H samples indicating a reduced degree of connectivity. Similarly, other studies reported an OP-related loss of transversal trabeculae that is responsible for a less interconnected structure and reduced mechanical performances (Ciarelli et al., 2000). OPen samples presented the highest variability of this parameter among the different anatomical regions, suggesting that structural modification due to osteoporosis onset could affect preferential anatomical sites of the humeral head.

By comparing the anatomical regions, no statistically significant differences were found among the morphometric parameters (Fig. 3). The only exception was found for the inferior biopsies that showed a reduced value of Tb.Sp compared to the central ones. Furthermore, even though not statistically significant, inferior biopsies presented higher Tb.Pf values, indicating a less connected structure. These results suggested that the inferior region could bear different loads, causing an alteration in the bone remodelling process and consequently leading to modification of structure porosity and connectivity.

Ciarelli et al. (2000), by analysing femoral biopsies through a micro-CT system, found morphological parameters similar to those of the present work (Tb.Th comprised between 100 and 150 μm and Po.To around 85%) and a significant increased DA for the fracture group compared to the control. In a more recent work, Vale et al. (2013) analysed trabecular bone biopsies harvested from OP femurs through a micro-CT system with a resolution of 30 μm. They obtained numerical values comparable to those of this work (Po.To around 87%, Tb.Sp around 750 μm). However, they found a higher Tb.Th value (210 μm) probably due to the higher loads that femurs should withstand, causing an increased remodelling rate. Comparable results were also obtained by Nikodem (2012) and by Zhang et al. (2010) by analysing femoral trabecular biopsies through micro-CT systems at a resolution of 20 and 36 μm, respectively. Ozan et al. (2017) used a micro-CT instrument to analyse the trabecular architecture of OP and OPen femoral biopsies obtaining comparable numerical values, even though they found different statistical variations between the two bone groups compared to this work. In fact, they reported that Tb.Sp was significantly lower in the OPen group while Po.To and Tb.Th was similar for the two groups.

It is fundamental to underline that morphometric parameters are strongly related to the resolution used in micro-CT analyses. In the literature, it is reported that Tb.Th is one of the most sensitive parameters to pixel size change (Isaksson et al., 2011; Kim et al., 2004). Consequently, OP samples analyses are influenced by the scan resolution, since their thinner trabeculae could be strongly overestimated by a low resolution. Higher pixel size could also lead to an overestimation of Tb.Sp if a high pixel size is associated with an inadequate binarisation threshold choice. Furthermore, thinner trabeculae present in the less loaded directions could disappear, leading to an increase of the DA value.

Thanks to the high resolution used in this study (equal to 3 μm) it is possible to confirm the high quality and reliability of the obtained morphometric parameters (summarised in Table 2).

3.2. Compression tests

Compression curves after a short region of pseudo linearity, ascribable to the elastic behaviour, presented a high fluctuating trend. Aleixo et al. (2012) by testing femoral trabecular biopsies, obtained curves with a similar trend and attributed this behaviour to a

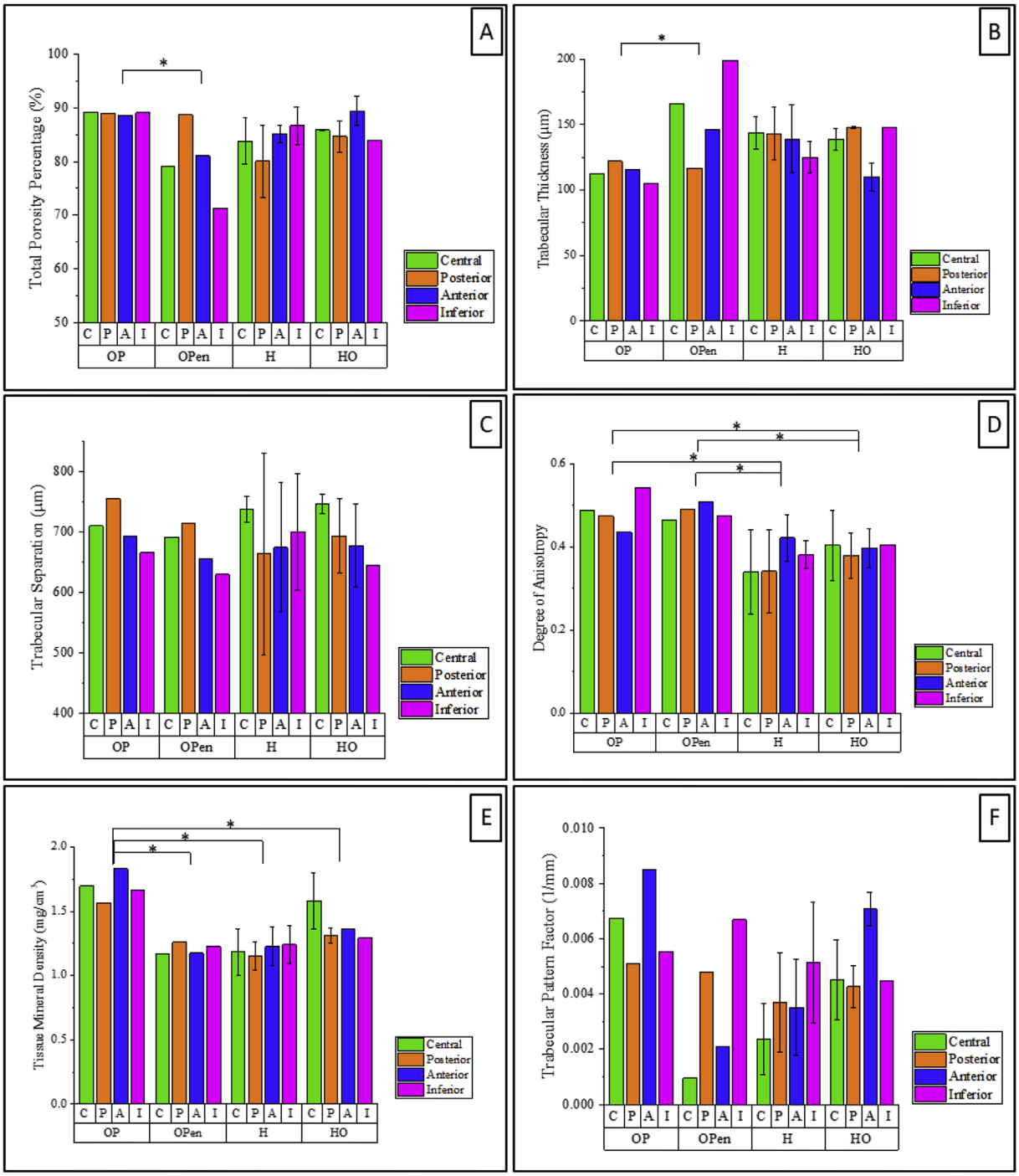


Fig. 2. Morphometric analyses subdivided according to groups. A) Total Porosity Percentage (Po.To), B) Trabecular Thickness (Tb.Th), C) Trabecular Separation (Tb.Sp), D) Degree of Anisotropy (DA), E) Tissue Mineral Density (TMD), F) Trabecular Pattern Factor (Tb.Pf). * corresponds to $p < 0.05$.

combination of plastic yielding, similar to that of cellular materials, and brittle fracture, due to trabeculae failure.

In order to obtain a mean numerical value of the stress in the fluctuating region, a non-linear fitting of the curves was performed and the stress measured at 30% strain was considered as the maximum stress withstood by bone trabeculae before their failure, adapting the procedure reported by Aleixo et al. in their work (Aleixo et al., 2012). Conversely to the cortical bone that is known to resist higher loads (Mirzaali et al., 2016), the failure stresses of trabecular bone structure tested in this work ranged between 1.2 and 3.3 MPa. These values are comparable with those obtained by other Authors concerning the mechanical testing of trabecular bone (Aleixo et al., 2012; Berot et al., 2012; Ciarallo et al., 2006; Li and Aspden, 1997; Ozan et al., 2017). Furthermore, a significant difference was found between OP samples and both H and HO ones (Fig. 4E), where the OP had inferior failure stresses.

Since bone is a composite material, it combines the toughness of the collagen matrix with the stiffness of the mineral phase. Consequently, alterations of both these components due to ageing and osteoporosis are expected to modify the bone mechanical properties (Fratzl et al., 2004). Nazarian et al. (2008) suggested that the inferior mechanical behaviour of OP bone found in their work was due to the creation of trabecular discontinuities by excessive osteoclast resorption. When the discontinuity affected transversal trabeculae, the remaining ones become

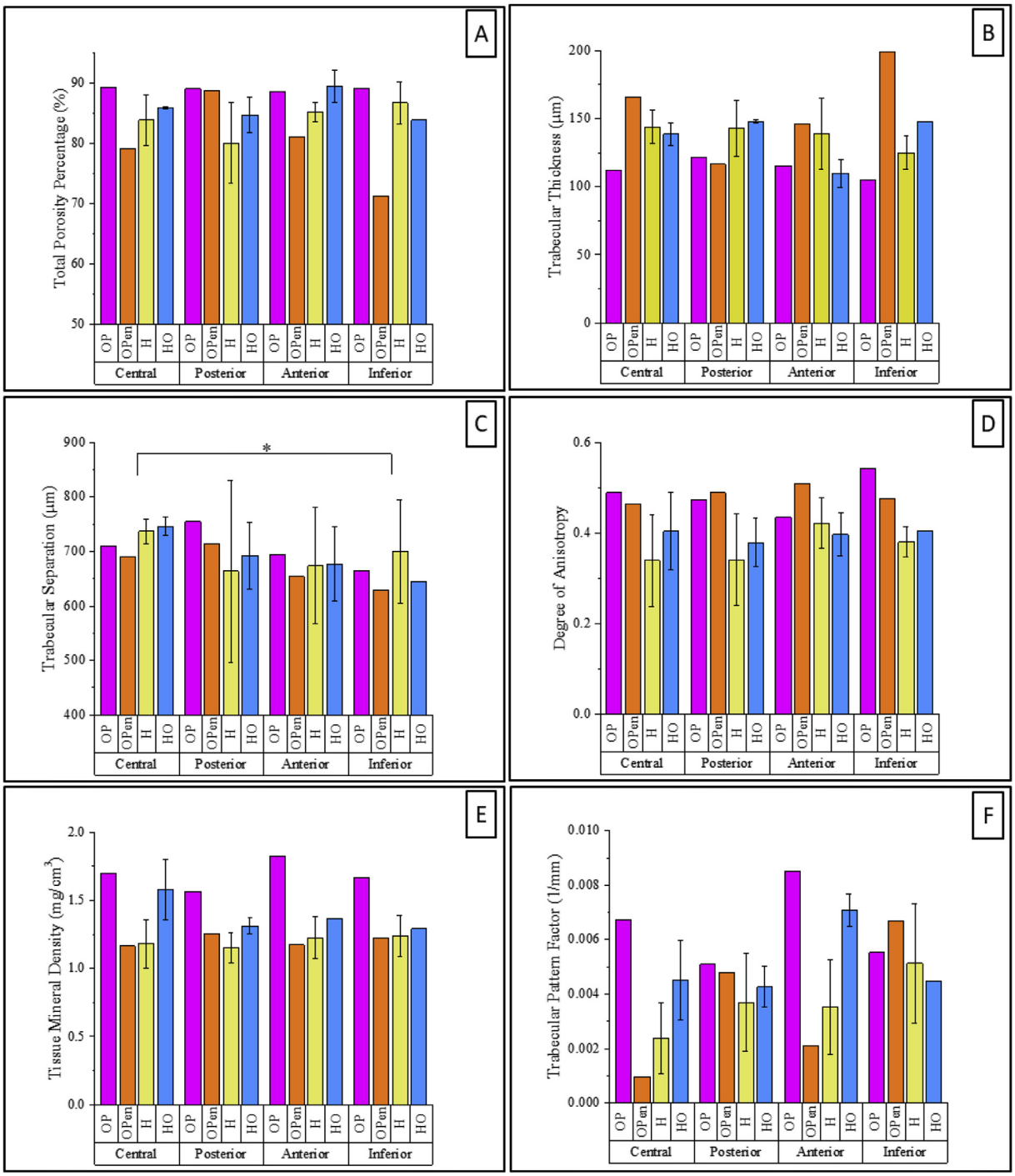


Fig. 3. Morphometric analyses subdivided according to the anatomical region. A) Total Porosity Percentage (Po.To), B) Trabecular Thickness (Tb.Th), C) Trabecular Separation (Tb.Sp), D) Degree of Anisotropy (DA), E) Tissue Mineral Density (TMD), F) Trabecular Pattern Factor (Tb.Pf). * corresponds to $p < 0.05$.

thinner and longer, with a consequent decreased stability. A similar mechanism can justify the inferior mechanical behaviour of the OP samples in this work. A statistical negative correlation was indeed found between the failure stresses and the Tb.Pf, a microstructural parameter corresponding to the inverse of structure connectivity (see section 3.7).

3.3. XRD analyses

In this work, HA crystallite size on *c*-axis was calculated by means of the Scherrer equation application on the XRD peak at 25.9 2θ degrees. The c-axis of biological HA corresponds to its longest axis and it is reported to be oriented parallel to the longitudinal axis of trabecular lamellae (Fratzl et al., 2004). OP samples presented the highest HA dimension (39.9 nm), while H samples the lowest one (24.3 nm ± 2.1 nm). OPen and HO samples showed intermediate crystallite values (31.9 nm for OPen and 30.1 nm ± 3.1 nm for HO). All values can be considered reliable since they are comparable to the size of biological HA reported in the literature (Fratzl et al., 2004; Rho et al., 1998). Differences between groups were all statistically significant (Fig. 5).

It is reported in the literature that the size of HA crystals can be

Table 2
Morphometric parameters calculated through micro-CT analysis.

Group	Zone	Po.To (%)	DA (none)	Tb.Th (μm)	Tb.Th SD (μm)	Tb.Sp (μm)	Tb.Sp SD (μm)	TMD (mg/cm^3)	Tb.Pf (1/mm)
OP	Central	89	0.49	112	39	710	215	1.70	0.0067
OPen	Central	79	0.46	166	56	690	219	1.17	0.0010
H	Central	84	0.34	144	49	737	245	1.18	0.0024
HO	Central	86	0.40	139	46	746	237	1.58	0.0045
OP	Posterior	89	0.47	122	44	754	240	1.57	0.0051
OPen	Posterior	89	0.49	117	42	714	205	1.26	0.0048
H	Posterior	80	0.34	143	55	663	262	1.15	0.0037
HO	Posterior	85	0.38	148	53	693	236	1.35	0.0043
OP	Anterior	89	0.43	116	40	693	212	1.83	0.0085
OPen	Anterior	81	0.51	146	58	654	220	1.17	0.0021
H	Anterior	85	0.42	139	49	674	217	1.23	0.0035
HO	Anterior	89	0.40	110	38	677	200	1.36	0.0071
OP	Inferior	89	0.54	105	35	665	190	1.67	0.0055
OPen	Inferior	71	0.48	199	69	629	222	1.20	0.0067
H	Inferior	87	0.38	125	40	700	250	1.24	0.0051
HO	Inferior	84	0.40	148	61	644	203	1.29	0.0045

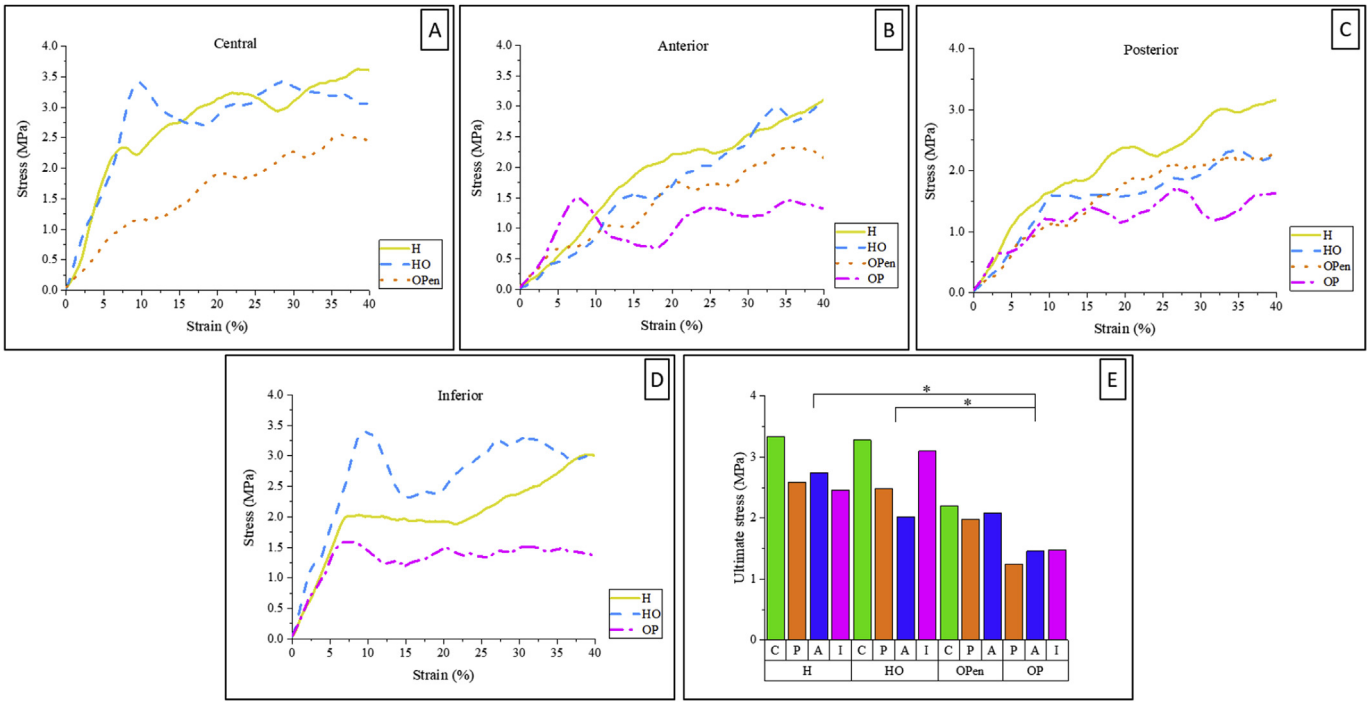


Fig. 4. Compression strain/stress curves of bone biopsies subdivided according to the anatomical region. A) Central, B) Anterior, C) Posterior and D) Inferior, E) Histogram of failure compressive strength measured at 30% strain. OP central and OPen inferior biopsies were not tested due to a reduced sample height. * corresponds to $p < 0.05$.

altered by the modification of the organic matrix and by other extrinsic factors such as ageing and diseases (Bala et al., 2013; Boskey, 2015). In particular, a recent work reported that OP could cause an increase in the presence of random coil collagen conformation (Pezzotti et al., 2017). Based on this finding, it is possible to hypothesise that the increased HA size found for OP samples in this work can be ascribed to a modification of the organic matrix. We suggest that a less organised collagen structure can lead to a less confined and controlled growth of HA crystals in OP samples. A similar modification, although to a lower extent, can be supposed for OPen and HO samples, who showed intermediate HA crystal dimensions. In addition, the larger HA crystals are hard to be resorbed by active osteoclasts and thus their relative amount can increase with ageing and OP presence. This observation is in good accordance with the results obtained by Gourion-Arsiquaud et al. (2009) who found that OP iliac crest biopsies possessed HA with higher crystallinity and larger dimensions. They hypothesised that the increased resorption rate of OP environment causes the preferential resorption of smaller HA crystals due to their higher solubility. In addition, they demonstrated that the increase in the mineral size had consequences at the mechanical level. Indeed, larger HA crystals cannot properly align to the collagen fibre matrix causing the weakening of the composite structure and consequently leading to an increased fracture risk. A similar behaviour was observed also in this study since a statistical correlation was found between failure stress and HA crystal size (see section 3.7).

3.4. Raman spectroscopy

The complete Raman spectra of healthy and OP samples are visible in Fig. 6. Several bands arising from the inorganic and organic components of bones can be detected. In particular, the spectra are dominated by the apatite phosphate groups symmetric stretching at 961 cm^{-1}, while the peak at 1070 cm^{-1} is evidence of the presence of carbonates. The main protein vibrational modes are instead located in

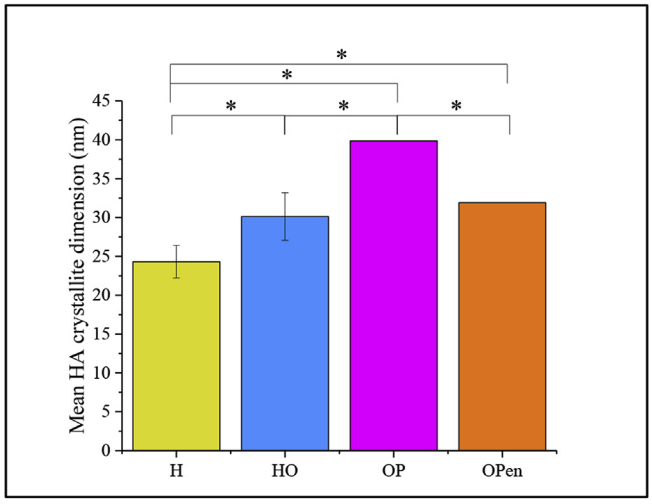


Fig. 5. HA crystallite dimension calculated through the Scherrer equation on XRD spectra. * corresponds to $p < 0.05$.

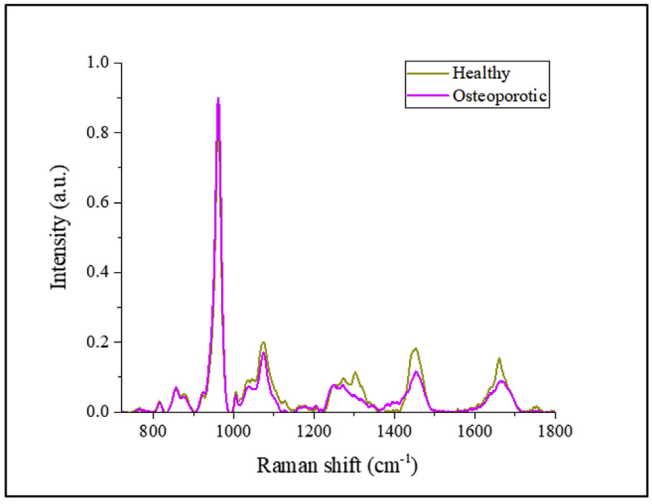


Fig. 6. Raman spectra of healthy and OP biopsies.

the ranges 1150-1350 cm^{-1} (amide III) and 1630-1690 cm^{-1} (amide I) and correspond to different vibrations of the peptide bonds, which are sensitive to the protein secondary structure. Some bands typical of single amino acids can be also recognised (phenylalanine 1005 cm^{-1}, 1582 cm^{-1}, 1608 cm^{-1}, proline 855 cm^{-1}).

Since the differences in the band intensity are affected by the scattering efficiency, laser penetration depth and other optical effects (Morris and Mandair, 2011), exclusively the peak areas and their ratios were analysed. No significant difference was evidenced by the analysis of the phosphate bands, thus only the amide I region was considered. Unfortunately, spectra were affected by the contribution of the bone marrow, particularly in healthy samples. This bone marrow contribution was also responsible for the spectral differences observed around 1300 cm^{-1} and 1440 cm^{-1}, where intense lipid bands do appear. By analysing the bone marrow as such, we could identify its main bands and evaluate its contribution to bone spectra.

In particular, within the amide I region (Fig. 7), random coil band at 1686 cm^{-1} presented an increased value of both full width at half maximum (FWHM) and area in OP samples compared to the healthy ones, indicating a stronger contribution of this collagen conformation. On the other hand, the area of the α-helix peak at 1666 cm^{-1} and that of the β-sheet peak at 1636 cm^{-1} decreased in OP samples. The area and FWHM values of the three different collagen conformations for both healthy and OP samples are resumed in Table 3. Based on these data it is possible to affirm that OP-induced a variation of collagen secondary structure toward a less organised conformation, that could be responsible for the increased HA crystal size found for OP samples. The literature reports indeed that the mineral crystal size could be influenced by the organic matrix properties, in addition to other intrinsic factors as the bone remodelling rate (Bala et al., 2013). Furthermore, the reduction of the α-helix contribution could be one of the reasons of the embrittlement of the OP bone. Actually, this specific conformation allows the protein to withstand larger plastic deformations, thanks to its mechanism of molecular unfolding by the reversible breaking of its hydrogen bonds (Pezzotti et al., 2017). Consequently, the lower presence of the α-helix conformation in OP samples could justify its altered mechanical and structural properties.

3.5. Nanoindentation tests

Nanoindentation tests performed on biopsies embedded in epoxy resin highlighted the elastic-plastic behaviour of bone samples (Oyen and Cook, 2009). The deformation, in fact, was not completely recovered after the removal of the load (Fig. 8). Through the application of the Oliver-Pharr method, reduced modulus and hardness values were calculated. The OP samples showed the highest values of E_r and H_c ($E_r = 16.15 \pm 0.70$ GPa, $H_c = 0.70 \pm 0.04$ GPa) compared to the other groups, but only the hardness was significantly different compared to H samples ($H_c = 0.47 \pm 0.05$ GPa), as visible in Fig. 6. These results were consistent with the increased values of TMD and HA crystal size of OP samples, as will be described in detail in section 3.7.

Tjhia et al. (2011) instead did not find differences in the mean values of E_r and H_c between healthy and OP samples, but they observed a reduced variation of hardness in the trabecular bone in OP samples. According to these Authors, this reduced heterogeneity in combination with an increased TMD led to a decreased resistance to crack propagation in OP bones that consequently caused reduced mechanical properties.

Fratzl-Zelman et al. (2009) found slightly higher values of E_r and H_c in OP samples compared to controls, but since they did not find an equivalent increase of calcium content as a mineral content indicator, they attributed this increase to a stiffening of the organic matrix in OP samples. Similarly, Bala et al. (2011) found a strong correlation between E_r and H_c with the collagen maturity degree.

While E_r and H_c distributions across bone osteons have been widely studied in the literature, reporting a reduction of E_r with increasing distance from the Haversian channel (Hengsberger et al., 2002), the distribution of these parameters across trabecular bone has been less investigated. Nanoindentation maps obtained in this work showed comparable distributions of E_r and H_c and no substantial variations were seen across the trabeculae thickness (Fig. 9). The embedding in resin caused the formation of a transition area, where E_r and H_c values progressively decreased, passing from bone to the resin. For this reason, nanoindentations performed at the bone-resin interface were not included in the data set for the calculation of the E_r and H_c previously reported.

3.6. Thermogravimetric analyses

TGA curves of all sample groups showed a similar pattern, characterised by three different steps of mass loss (Fig. 10). The first loss occurred between 100° and 150 °C and is attributable to the desorption of water. Since samples were previously dehydrated in order to be hand-crushed and obtain a powder, the amount of mass loss in this phase is only 5–10%, lower than the one usually reported in the literature (Charmas, 2013; Lau et al., 2013). From 300° to 500 °C, a second mass loss was registered due to the decomposition of the organic matrix that represented between 30 and 35% of the bone mass. In addition in this range, a change of slope above 350 °C is attributable to the

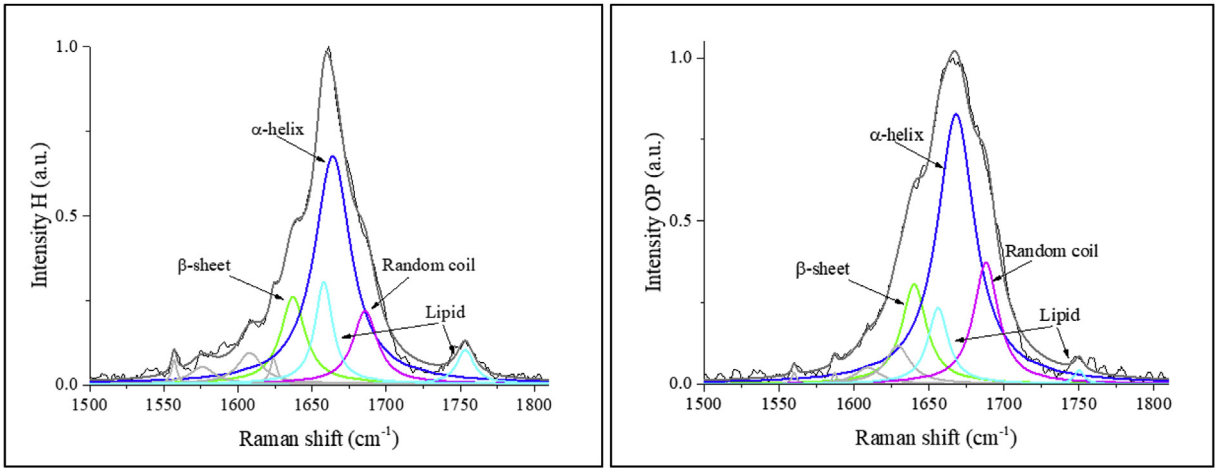


Fig. 7. Raman spectra of the amide I region of healthy (left) and OP biopsies (right).

Table 3
Area and FWHM values of collagen conformations of healthy and OP biopsies extrapolated from Raman spectra.

Collagen Conformation	Raman Shift (cm^{-1})	Area H (%)	Area OP (%)	FWHM H (cm^{-1})	FWHM OP (cm^{-1})
β-sheet	1636	14.7	15.4	20.1	19.3
α-helix	1666	49.5	43.6	26.8	27.5
Random coil	1686	11.2	16.2	18.3	24.7

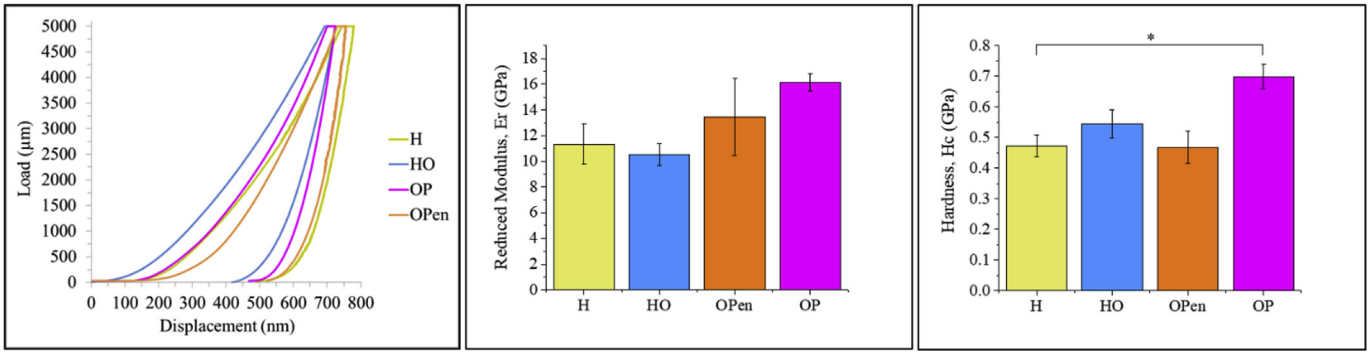


Fig. 8. Representative nanoindentation curves (left), Reduced Modulus values (middle) and Hardness values of bone biopsies. * corresponds to $p < 0.05$.

decomposition of the carbonate species (Mkukuma et al., 2005). Above 600 °C no further mass changes were registered since the decomposition of the residual inorganic phase is expected above 850 °C (Lau et al., 2013).

By comparing the different groups is possible to observe that a higher amount of residual water was present in the OP and HO samples compared to the H ones (Table 4). Charmas (2013) attributed this behaviour to the ability of larger pores present in OP bones to adsorb higher amount of water. The inorganic and organic fractions instead were not significantly different between OP and H samples, as reported also by Li and Aspen (Li and Aspden, 1997).

Except for the water contribution, H and OP samples showed similar organic to inorganic phase ratio: organic components represented the 35% while the inorganic ones the 65% (Table 5). Only HO samples showed a decreased amount of inorganic phase (60%), while OPen samples had an intermediate behaviour, showing 63% of the inorganic phase. TGA data did not highlight an increase in the mineralisation degree of OP bone, contrarily to what evidenced by TMD measurements. TGA, however, allowed measuring the mean composition of trabecular bone, while TMD was performed on individual trabeculae. For this reason, the difference between OP and H composition cannot be clearly evidenced by TGA measurements. In addition, the defatting treatment performed prior to TGA analysis could reduce the organic phase amount and consequently modify the organic-to-inorganic ratio.

3.7. Correlation between structural and mechanical parameters

Concerning morphological parameters, Pearson's correlation analyses showed a significant negative correlation between total porosity percentage (Po.To) and trabecular thickness (Tb.Th) (Pearson = −0.814, p-value = 0.001), confirming that the reduction of trabecular thickness is associated with an increase of the porosity. Regression analysis showed a linear dependence of these parameters (Fig. 11A).

A positive strong correlation was also found between contact hardness and reduced modulus (Pearson = 0.826, p-value = 0.003), as already supposed from nanoindentation maps which showed a comparable distribution of those parameters. A linear relationship between those parameters in bone was already reported in the literature (Oyen, 2006).

By comparing morphological and mechanical parameters at the microscopic level, the only significant correlation was found between TMD and H_c (Fig. 11C). This positive moderate correlation (Pearson = 0.685 and p-value = 0.014) suggested that the increase of

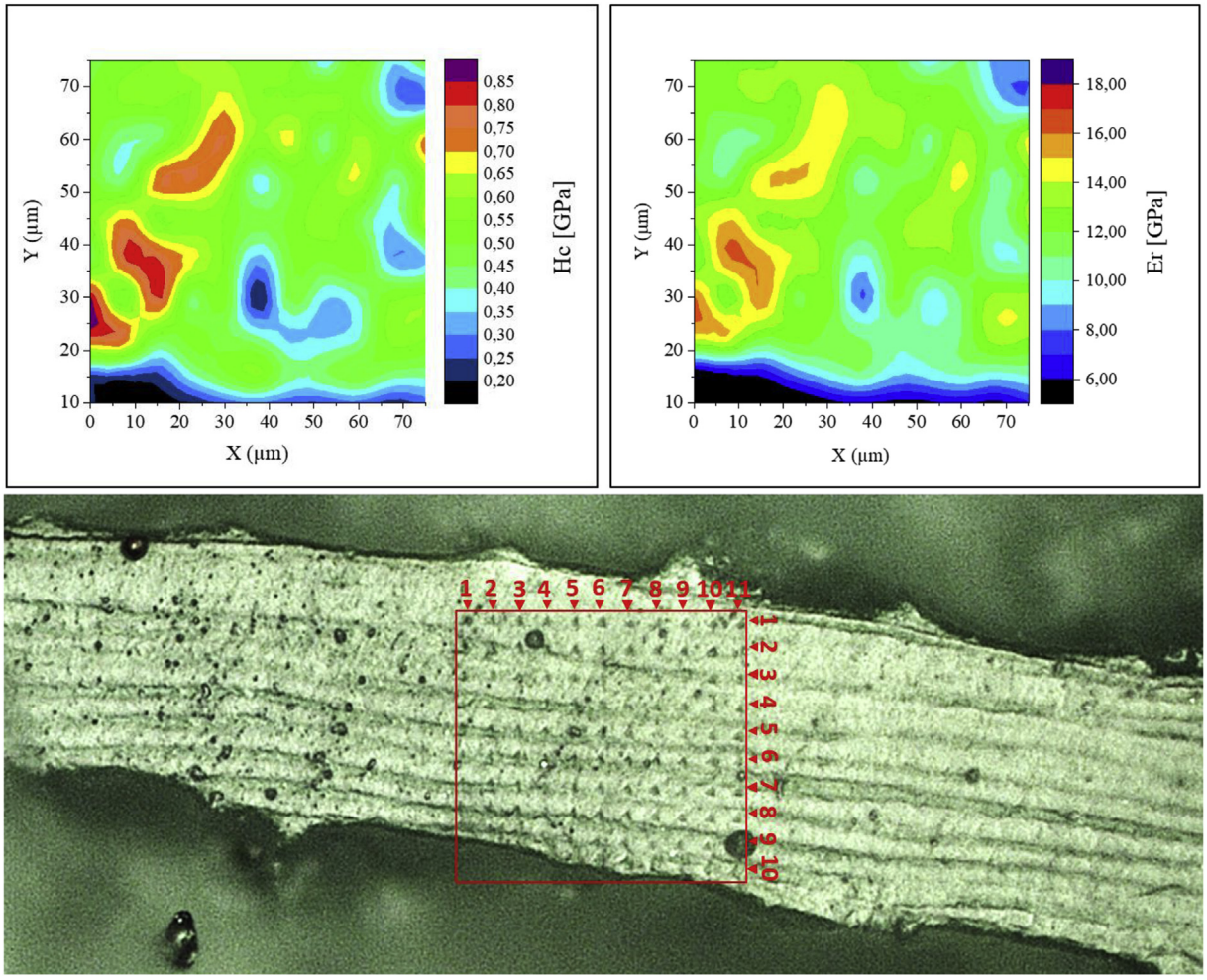


Fig. 9. Maps of Hardness and Reduced Modulus on a bone trabecula (top) and SEM image of the nanoindentation area (bottom).

TMD observed in OP samples is associated with an increased hardness value, probably due to the reduced deformation ability of the denser and more mineralised trabeculae.

HA crystallite dimensions calculated through XRD analyses showed a positive correlation with both H_c and E_r (Pearson = 0.721 and p-value = 0.008 and Pearson = 0.605 and p-value = 0.037, respectively) and with TMD (Pearson = 0.604 and p-value = 0.038). These results suggested that the increase of HA crystallite dimension measured for OP

Table 4
bone sample composition extrapolated from TGA data.

Mass Loss %	OP	H	HO	OPen
Water	8%	5%	8%	5%
Organic phase	40%	39%	44%	40%
Inorganic phase	52%	56%	48%	55%

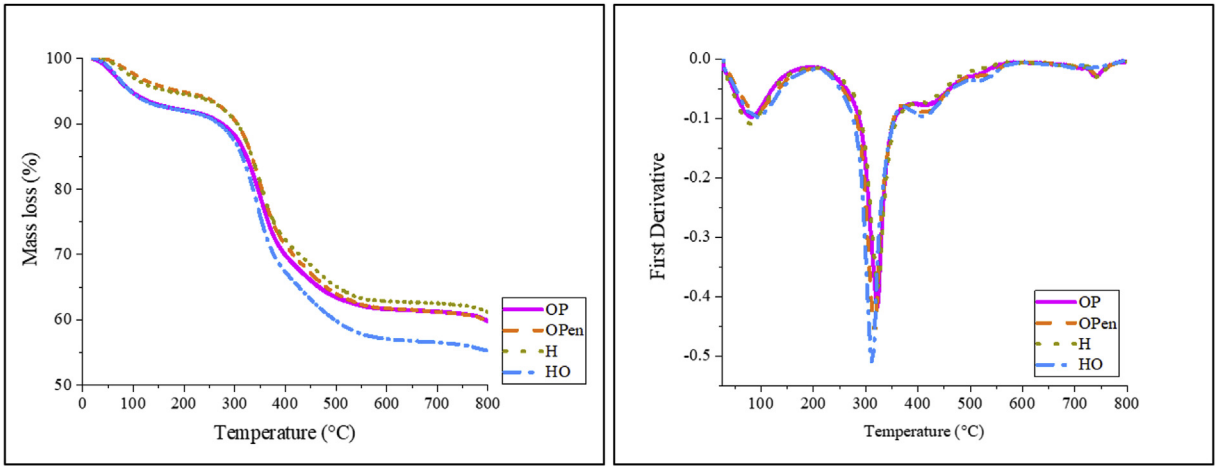


Fig. 10. Thermogravimetric curves of bone biopsies (right) and their first derivative (left).

Table 5
bone sample composition extrapolated from TGA data excluding water contribution.

Mass loss % without water	OP	H	HO	OPen
Organic phase	35%	35%	40%	37%
Inorganic phase	65%	65%	60%	63%

sample was accompanied by increased mechanical properties and by an increased density of trabecular bone. The relationship between these parameters was linear and it is visible in Fig. 11D–F. Bala and Seeman (2015), by testing iliac bone samples, contrarily did not find any correlations between HA crystal size and the nanoindentation parameters. In their work, E_r and H_c were instead correlated with BMD, calculated from the grey level of micro-radiographic digital images, and collagen maturity, measured through FTIR peak analysis. Similarly, Nazarian et al. (2008) did not find significant differences between OP and H samples in the nanoindentation parameters, TMD or mineral content measured on spinal and proximal femoral biopsies. They reported that only bone volume fraction was a predictive index of mechanical properties at the microscale.

A negative correlation was instead found between the compressive failure stress and HA crystallite dimension (Pearson = −0.769 and p-value = 0.003) and with TMD (Pearson = −0.594 and p-value = 0.042). Therefore, the increase of the mean mineral particle length and the level of trabecular mineralisation make the bone matrix stiffer and less resistant to loads, as already reported in the literature (Bala and Seeman, 2015; Fratzl et al., 2004; Osterhoff et al., 2016). OP bone, which presented the highest TMD and the highest HA crystal dimension, in fact, showed the lowest ultimate stress values from compression tests.

The compressive failure stress correlated negatively also with the Tb.Pf, an inverse index of trabecular connectivity (Pearson = −0.611 and p-value = 0.035). OP samples who withstood inferior compressive loads, showed, in fact, lower connectivity, even though not statistically significant. The reduction of trabecular connectivity is an intrinsic feature of OP disease which causes the alteration of bone structure and, in particular, the disruption of transversal trabeculae (Brandi, 2009).

No other correlations were found between micro-CT parameters and the macroscopic mechanical behaviour of bone biopsies in this work. Similarly, Osterhoff et al. (2016) reported a more significant influence of trabecular connectivity on bone biomechanical strength than other micro-architectural parameters, such as the trabecular thickness or the bone mineral density. However, in the literature, a high number of research studies found a statistically significant relationship between bone strength and bone volume fraction (Berot et al., 2012; Ciarallo et al., 2006; Ciarelli et al., 2000). All Pearson's coefficients found by the correlation analyses performed in this work are resumed in Table 6.

The complete characterisation of bone tissue across different scale lengths is a complex, still open field of research and further studies are needed to find correlations between parameters arising from different analytical techniques. Once these correlations will be univocally

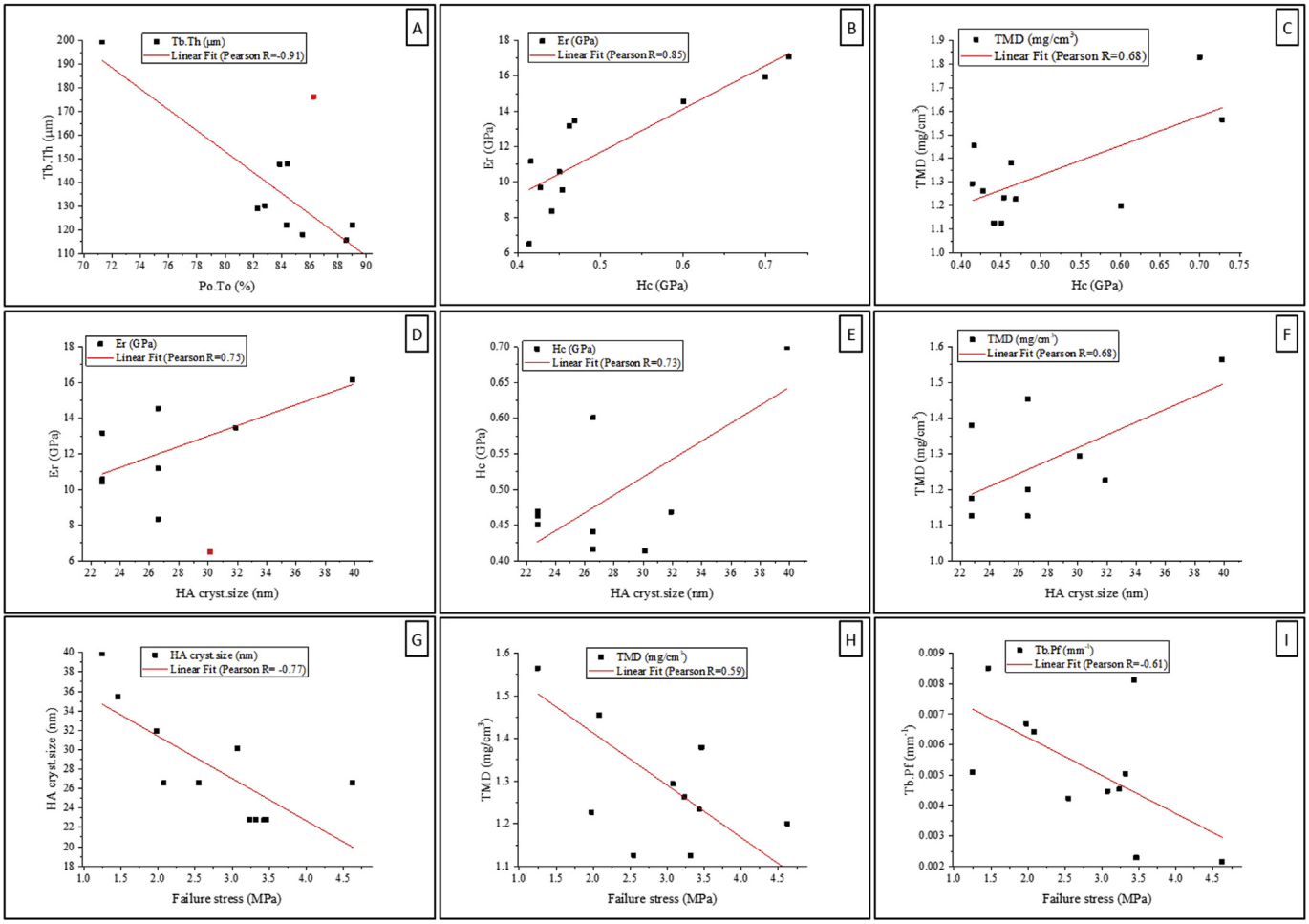


Fig. 11. Linear regression of parameters that showed significant correlations according to Pearson analysis. A) Po.To vs Tb.Th; B) Er vs H_c, C) H_c vs TMD; D) HA crystallite size vs E_r; E) HA crystallite size vs H_c; F) HA crystallite size vs TMD; G) Ultimate stress vs HA crystallite size; H) Ultimate stress vs TMD; I) Ultimate stress vs Tb.Pf.

Table 6
Pearson's correlation coefficients and p-values.

		HA cryst.size	E_r	H_c	Po.To	DA	Tb.Th	Tb.Sp	TMD	Tb.Pf	$б_f$
HA cryst. size	Pearson Cor.	1	**0.605**	**0.721**	−0.106	0.241	0.220	0.152	**0.604**	0.329	**−0.769**
	p-value	–	**0.037**	**0.008**	0.743	0.450	0.492	0.638	**0.038**	0.296	**0.003**
E_r	Pearson Cor.	**0.605**	1	**0.826**	−0.108	0.360	−0.091	0.063	0.576	0.097	−0.391
	p-value	**0.037**	–	**0.001**	0.737	0.250	0.780	0.847	0.050	0.764	0.209
H_c	Pearson Cor.	**0.721**	**0.826**	1	0.316	0.120	−0.358	0.193	**0.685**	0.113	−0.371
	p-value	**0.008**	**0.001**	–	0.317	0.711	0.254	0.548	**0.014**	0.727	0.235
Porosity	Pearson Cor.	−0.106	−0.108	0.316	1	−0.307	**−0.840**	0.427	0.347	0.015	0.144
	p-value	0.743	0.737	0.317	–	0.332	**0.001**	0.167	0.269	0.964	0.655
DA	Pearson Cor.	0.241	0.360	0.120	−0.307	1	0.276	0.328	0.239	−0.240	−0.283
	p-value	0.450	0.250	0.711	0.332	–	0.385	0.298	0.455	0.453	0.373
Tb.Th	Pearson Cor.	0.220	−0.091	−0.358	**−0.840**	0.276	1	−0.024	−0.367	0.089	−0.349
	p-value	0.492	0.780	0.254	**0.001**	0.385	–	0.941	0.240	0.783	0.267
Tb.Sp	Pearson Cor.	0.152	0.063	0.193	0.427	0.328	−0.024	1	0.233	−0.072	−0.208
	p-value	0.638	0.847	0.548	0.167	0.298	0.941	–	0.465	0.825	0.516
TMD	Pearson Cor.	**0.604**	0.576	**0.685**	0.347	0.239	−0.367	0.233	1	0.385	**−0.594**
	p-value	**0.038**	0.050	**0.014**	0.269	0.455	0.240	0.465	–	0.217	**0.042**
Tb.Pf	Pearson Cor.	0.329	0.097	0.113	0.015	−0.240	0.089	−0.072	0.385	1	**−0.611**
	p-value	0.296	0.764	0.727	0.964	0.453	0.783	0.825	0.217	–	**0.035**
$б_f$	Pearson Cor.	**−0.769**	−0.391	−0.371	0.144	−0.283	−0.349	−0.208	**−0.594**	**−0.611**	1
	p-value	**0.003**	0.209	0.235	0.655	0.373	0.267	0.516	**0.042**	**0.035**	–

identified, they can be usefully employed for the assessment of disease-related modifications and consequently for OP diagnosis.

3.8. Limitations

Concerning the limitations of this work, it is essential to mention the limited number of bone samples. Since bones were derived from patients undergoing an intervention of shoulder arthroplasty, the number of the collected samples depended primarily on the willingness of the patient to donate and on his/her compliance with the recruiting protocol. This was particularly limiting for OP samples. Since we were interested in the analysis of OP-related bone architecture changes, only OP samples from patients not under drug therapy were selected, as anti-osteoporotic drug therapy is associated with bone structure modification (Gallacher and Dixon, 2010; Schafer et al., 2013). This condition was hard to find since drug treatment is the gold standard for osteoporosis therapy and anabolic or anti-resorptive agents are largely administered after its diagnosis. Consequently, the number of suitable OP donors was very small.

Since the number of samples has a strong influence on the sensitivity of the statistical analyses outcomes, the conclusions reported in this work would be more reliable if a higher number of samples was collected. Unfortunately, the collection of biological samples is usually an inherently weak, not fully predictable process, that does not always lead to the number of samples needed to perform powerful statistical analyses.

Furthermore, the humeral head quality was strongly affected by the execution of the arthroplasty surgical procedure, that sometimes led to discard some biopsies since the harvested area had reduced bone quality.

However, the results obtained in this work can introduce new important insights into the OP-induced variations of trabecular features in the humeral heads.

Another limitation of this study is NBF fixation and ethanol conservation, which are reported to alter the mechanical properties of the organic matrix leading to the stiffening of bone structure (Hammer et al., 2014; Vesper et al., 2017). However, all sample groups were subjected to the same treatment, thus comparisons between them can be considered reliable.

4. Conclusions

Morphological, structural and mechanical analyses of cylindrical bone biopsies harvested from human humeral heads were performed, in order to assess possible OP-related modifications of bone properties. Morphological analyses conducted through a high-resolution micro-CT revealed a statistically significant increase of anisotropy and of TMD in OP samples, while no statistical differences among groups were found concerning the other micro-CT parameters and among the different anatomical regions of the proximal humeral head. Only biopsies belonging to the inferior region showed a reduced trabecular separation compared to the central ones. The architectural modifications of OP samples decreased their mechanical strength to compression loads, mainly due to their reduced trabecular connectivity.

HA crystallite size, calculated through the application of the Scherrer equation to XRD spectra, was higher for OP samples and was statistically correlated with TMD values. OP samples showed also increased E_r and H_c values extrapolated from nanoindentation tests. The latter parameter was significantly different compared to H samples and showed a linear correlation with both HA crystallite size and TMD values. These results suggest that OP causes an increased HA crystal growth, mostly ascribed to a modified organisation of the organic matrix. The alteration of the bone organic structure was confirmed by Raman spectroscopy, that showed an increased contribution of random coil conformation of collagen molecules in OP samples. This less organised structure could be responsible for the less confined growth of HA crystals in OP bone trabeculae and consequently to a reduced deformation capability under nanoindentation load. The increased degree of mineralisation of OP trabeculae is also responsible for their reduced macroscopic mechanical strength since higher mineralised trabeculae are more brittle and can withstand reduced compressive loads before their failure.

In conclusion, it is possible to confirm that OP affects bone properties at different scale lengths causing an alteration of its morphological, structural and mechanical features.

Funding

This project has received funding from the European Research Council (ERC) under the European Union's Horizon 2020 research and innovation programme (grant agreement No 681798-BOOST) (www.ercprojectboost.eu).

Declarations of interest

None.

Acknowledgements

The authors would like to thanks the Head of Shoulder and Elbow Unit of Istituto Ortopedico Rizzoli, Prof. Roberto Rotini for bone protocol approval.

References

Aleixo, I., Vale, A.C., Lúcio, M., Amaral, P.M., Rosa, L.G., Caetano-Lopes, J., Rodrigues, A., Canhão, H., Fonseca, J.E., Vaz, M.F., 2012. A method for the evaluation of femoral head trabecular bone compressive properties. Mater. Sci. Forum 730–732, 3–8. https://doi.org/10.4028/www.scientific.net/MSF.730-732.3.

Alidousti, H., Giles, J.W., Emery, R.J.H., Jeffers, J., 2017. Spatial mapping of humeral head bone density. J. Shoulder Elb. Surg. 26, 1653–1661. https://doi.org/10.1016/j.jse.2017.03.006.

Bala, Y., Depalle, B., Douillard, T., Meille, S., Clément, P., Follet, H., Chevalier, J., Boivin, G., 2011. Respective roles of organic and mineral components of human cortical bone matrix in micromechanical behavior: an instrumented indentation study. J. Mech. Behav. Biomed. Mater. 4, 1473–1482. https://doi.org/10.1016/j.jmbbm.2011.05.017.

Bala, Y., Farlay, D., Boivin, G., 2013. Bone mineralization: from tissue to crystal in normal and pathological contexts. Osteoporos. Int. 24, 2153–2166. https://doi.org/10.1007/s00198-012-2228-y.

Bala, Y., Seeman, E., 2015. Bone's material constituents and their contribution to bone strength in health, disease, and treatment. Calcif. Tissue Int. 97, 308–326. https://doi.org/10.1007/s00223-015-9971-y.

Barvencik, F., Gebauer, M., Beil, F.T., Vettorazzi, E., Mumme, M., Rupprecht, M., Pogoda, P., Wegscheider, K., Rueger, J.M., Pueschel, K., Amling, M., 2010. Age- and sex-related changes of humeral head microarchitecture: histomorphometric analysis of 60 human specimens. J. Orthop. Res. 28, 18–26. https://doi.org/10.1002/jor.20957.

Berot, M., Auregan, J.-C., Imbert, L., Magoariec, H., Budyn, E., Zadegan, F., Hannouche, D., Bensidhoum, M., Hoc, T., 2012. Mechanics of osteoporotic trabecular bone. Mec. Ind. 13, 373–380. https://doi.org/10.1051/meca/2012023.

Boskey, A.L., 2015. Bone composition: relationship to bone fragility and anti-osteoporotic drug effects. BoneKEy Rep. 4, 1–11. https://doi.org/10.1038/bonekey.2015.79.

Brandi, M.L., 2009. Microarchitecture, the key to bone quality. Rheumatology 48 (4), iv3–iv8. (United Kingdom) 48. https://doi.org/10.1093/rheumatology/kep273.

Charmas, B., 2013. TG and DSC studies of bone tissue: effects of osteoporosis. Thermochim. Acta 573, 73–81. https://doi.org/10.1016/j.tca.2013.08.032.

Chen, H., 2014. Bone three-dimensional microstructural features of the common osteoporotic fracture sites. World J. Orthop. 5, 486. https://doi.org/10.5312/wjo.v5.i4.486.

Ciarallo, A., Barralet, J., Tanzer, M., Kremer, R., 2006. An approach to compare the quality of cancellous bone from the femoral necks of healthy and osteoporotic patients through compression testing and microcomputed tomography imaging. McGill J. Med. 9, 102–107. https://doi.org/10.3103/S0096392510040243.

Ciarelli, T.E., Fyhrie, D.P., Schaffler, M.B., Goldstein, S.A., 2000. Variations in three-dimensional cancellous bone architecture of the proximal femur in female hip fractures and in controls. J. Bone Miner. Res. 15, 32–40. https://doi.org/10.1359/jbmr.2000.15.1.32.

Dimai, H.P., 2017. Use of dual-energy X-ray absorptiometry (DXA) for diagnosis and fracture risk assessment; WHO-criteria, T- and Z-score, and reference databases. Bone 104, 39–43. https://doi.org/10.1016/j.bone.2016.12.016.

Fathi, M.H., Hanifi, A., Mortazavi, V., 2008. Preparation and bioactivity evaluation of bone-like hydroxyapatite nanopowder. J. Mater. Process. Technol. 202, 536–542. https://doi.org/10.1016/j.jmatprotec.2007.10.004.

Fratzl-Zelman, N., Roschger, P., Gourrier, A., Weber, M., Misof, B.M., Loveridge, N., Reeve, J., Klaushofer, K., Fratzl, P., 2009. Combination of nanoindentation and quantitative backscattered electron imaging revealed altered bone material properties associated with femoral neck fragility. Calcif. Tissue Int. 85, 335–343. https://doi.org/10.1007/s00223-009-9289-8.

Fratzl, P., Gupta, H.S., Paschalis, E.P., Roschger, P., 2004. Structure and mechanical quality of the collagen-mineral nano-composite in bone. J. Mater. Chem. 14, 2115–2123. https://doi.org/10.1039/b402005g.

Gallacher, S.J., Dixon, T., 2010. Impact of treatments for postmenopausal osteoporosis (bisphosphonates, parathyroid hormone, strontium ranelate, and denosumab) on bone quality: a systematic review. Calcif. Tissue Int. 87, 469–484. https://doi.org/10.1007/s00223-010-9420-x.

Genant, H.K., Engelke, K., Prevrhal, S., 2008. Advanced CT bone imaging in osteoporosis. Rheumatology 47. https://doi.org/10.1093/rheumatology/ken180.

Glowacki, J., Vokes, T., 2016. Osteoporosis and mechanisms of skeletal aging. In: Sierra, F., Kohanski, R. (Eds.), Advances in Geroscience. Springer International Publishing, Cham, pp. 277–307. https://doi.org/10.1007/978-3-319-23246-1_10.

Gourion-Arsiquaud, S., Faibish, D., Myers, E., Spevak, L., Compston, J., Hodsman, A., Shane, E., Recker, R.R., Boskey, E.R., Boskey, A.L., 2009. Use of FTIR spectroscopic imaging to identify parameters associated with fragility fracture. J. Bone Miner. Res. 24, 1565–1571. https://doi.org/10.1359/jbmr.090414.

Hammer, N., Voigt, C., Werner, M., Hoffmann, F., Bente, K., Kunze, H., Scholz, R., Steinke, H., 2014. Ethanol and formaldehyde fixation irreversibly alter bones' organic matrix. J. Mech. Behav. Biomed. Mater. 29, 252–258. https://doi.org/10.1016/j.jmbbm.2013.09.008.

Hengsberger, S., Kulik, A., Zysset, P. h., 2002. Nanoindentation discriminates the elastic properties of individual human bone lamellae under dry and physiological conditions. Bone 30, 178–184. https://doi.org/10.1016/S8756-3282(01)00624-X.

Hepp, P., Lill, H., Bail, H., Korner, J., Niederhagen, M., Haas, N.P., Josten, C., Duda, G.N., 2003. Where should implants Be anchored in the humeral head? Clin. Orthop. Relat. Res. 139–147. https://doi.org/10.1097/01.blo.0000092968.12414.a8.

Isaksson, H., Töyräs, J., Hakulinen, M., Aula, A.S., Tamminen, I., Julkunen, P., Kröger, H., Jurvelin, J.S., 2011. Structural parameters of normal and osteoporotic human trabecular bone are affected differently by microCT image resolution. Osteoporos. Int. 22, 167–177. https://doi.org/10.1007/s00198-010-1219-0.

Kim, D.G., Christopherson, G.T., Dong, X.N., Fyhrie, D.P., Yeni, Y.N., 2004. The effect of microcomputed tomography scanning and reconstruction voxel size on the accuracy of stereological measurements in human cancellous bone. Bone 35, 1375–1382. https://doi.org/10.1016/j.bone.2004.09.007.

Lau, M.L., Lau, K.T., Ku, H., Cardona, F., Lee, J.H., 2013. Analysis of heat-treated bovine cortical bone by thermal gravimetric and nanoindentation. Compos. B Eng. 55, 447–452. https://doi.org/10.1016/j.compositesb.2013.06.027.

Launonen, A.P., Lepola, V., Saranko, A., Flinkkilä, T., Laitinen, M., Mattila, V.M., 2015. Epidemiology of proximal humerus fractures. Arch. Osteoporos. 10, 1–5. https://doi.org/10.1007/s11657-015-0209-4.

Li, B., Aspden, R.M., 1997. Composition and mechanical properties of cancellous bone from the femoral head of patients with osteoporosis or osteoarthritis. J. Bone Miner. Res. 12, 641–651. https://doi.org/10.1359/jbmr.1997.12.4.641.

Lloyd, A.A., Wang, Z.X., Donnelly, E., 2015. Multiscale contribution of bone tissue material property heterogeneity to trabecular bone mechanical behavior. J. Biomech. Eng. 137, 010801. https://doi.org/10.1115/1.4029046.

Mantila Roosa, S.M., Hurd, A.L., Xu, H., Fuchs, R.K., Warden, S.J., 2012. Age-related changes in proximal humerus bone health in healthy, white males. Osteoporos. Int. 23, 2775–2783. https://doi.org/10.1007/s00198-012-1893-1.

Mirzaali, M.J., Schwiedrzik, J.J., Thaiwichai, S., Best, J.P., Michler, J., Zysset, P.K., Wolfram, U., 2016. Mechanical properties of cortical bone and their relationships with age, gender, composition and microindentation properties in the elderly. Bone 93, 196–211. https://doi.org/10.1016/j.bone.2015.11.018.

Mkukuma, L.D., Imrie, C.T., Skakle, J.M.S., Hukins, D.W.L., Aspden, R.M., 2005. Thermal stability and structure of cancellous bone mineral from the femoral head of patients with osteoarthritis or osteoporosis. Ann. Rheum. Dis. 64, 222–225. https://doi.org/10.1136/ard.2004.021329.

Morris, M.D., Mandair, G.S., 2011. Raman assessment of bone quality. Clin. Orthop. Relat. Res. 469, 2160–2169. https://doi.org/10.1007/s11999-010-1692-y.

Nazarian, A., Von Stechow, D., Zurakowski, D., Müller, R., Snyder, B.D., 2008. Bone volume fraction explains the variation in strength and stiffness of cancellous bone affected by metastatic cancer and osteoporosis. Calcif. Tissue Int. 83, 368–379. https://doi.org/10.1007/s00223-008-9174-x.

Nikodem, A., 2012. Correlations between structural and mechanical properties of human trabecular femur bone. Acta Bioeng. Biomech. 14, 37–46. https://doi.org/10.5277/abb120205.

Oliver, W.C., Pharr, G.M., 1992. An improved technique for determining hardness and elastic modulus using load and displacement sensing indentation experiments. J. Mater. Res. 7 (6), 1564–1583. https://doi.org/10.1557/JMR.1992.1564.

Osterhoff, G., Morgan, E.F., Shefelbine, S.J., Karim, L., McNamara, L.M., Augat, P., 2016. Bone mechanical properties and changes with osteoporosis. Injury 47, S11–S20. https://doi.org/10.1016/S0020-1383(16)47003-8.

Oyen, M.L., 2006. Nanoindentation hardness of mineralized tissues. J. Biomech. 39, 2699–2702. https://doi.org/10.1016/j.jbiomech.2005.09.011.

Oyen, M.L., Cook, R.F., 2009. A practical guide for analysis of nanoindentation data. J. Mech. Behav. Biomed. Mater. 2, 396–407. https://doi.org/10.1016/j.jmbbm.2008.10.002.

Ozan, F., Pekedis, M., Koyuncu, Ş., Altay, T., Yıldız, H., Kayalı, C., 2017. Micro-computed tomography and mechanical evaluation of trabecular bone structure in osteopenic and osteoporotic fractures. J. Orthop. Surg. 25. https://doi.org/10.1177/2309499017692718.

Pezzotti, G., Rondinella, A., Marin, E., Zhu, W., Aldini, N.N., Ulian, G., Valdrè, G., 2017. Raman spectroscopic investigation on the molecular structure of apatite and collagen in osteoporotic cortical bone. J. Mech. Behav. Biomed. Mater. 65, 264–273. https://doi.org/10.1016/j.jmbbm.2016.08.030.

Rho, J.Y., Hobatho, M.C., A, R.B., 1995. Relations of mechanical properties to density and CT numbers in human bone. Med. Eng. Phys. 17, 347–355. https://doi.org/10.1016/1350-4533(95)97314-F.

Rho, J.Y., Kuhn-Spearing, L., Zioupos, P., 1998. Mechanical properties and the hierarchical structure of bone. Med. Eng. Phys. 20, 92–102. https://doi.org/10.1016/S1350-4533(98)00007-1.

Saitoh, S., Nakatsuchi, Y., Latta, L., Milne, E., 1994. Distribution of bone mineral density and bone strength of the proximal humerus. J. Shoulder Elb. Surg. 3, 234–242. https://doi.org/10.1016/S1058-2746(09)80041-4.

Schafer, A.L., Burghardt, A.J., Sellmeyer, D.E., Palermo, L., Shoback, D.M., Majumdar, S., Black, D.M., 2013. Postmenopausal women treated with combination parathyroid hormone (1-84) and ibandronate demonstrate different microstructural changes at the radius vs. tibia: the PTH and Ibandronate Combination Study (PICS). Osteoporos. Int. 24, 2591–2601. https://doi.org/10.1007/s00198-013-2349-y.

Sprecher, C.M., Schmidutz, F., Helfen, T., Geoff Richards, R., Blauth, M., Milz, S., 2015. Histomorphometric assessment of cancellous and cortical bone material distribution in the proximal humerus of normal and osteoporotic individuals: significantly reduced bone stock in the metaphyseal and subcapital regions of osteoporotic individuals. Med. (United States) 94, 1–7. https://doi.org/10.1097/MD.0000000000002043.

Stauber, M., Müller, R., 2006. Age-related changes in trabecular bone microstructures: global and local morphometry. Osteoporos. Int. 17, 616–626. https://doi.org/10.1007/s00198-005-0025-6.

Sterling, J.A., Guelcher, S.A., 2014. Biomaterial scaffolds for treating osteoporotic bone. Curr. Osteoporos. Rep. 12, 48–54. https://doi.org/10.1007/s11914-014-0187-2.

Tingart, M.J., Bouxsein, M.L., Zurakowski, D., Warner, J.P., Apreleva, M., 2003. Three-Dimensional distribution of bone density in the proximal humerus. Calcif. Tissue Int. 73, 531–536. https://doi.org/10.1007/s00223-002-0013-9.

Tjhia, C.K., Odvina, C.V., Rao, D.S., Stover, S.M., Wang, X., Fyhrie, D.P., 2011. Mechanical property and tissue mineral density differences among severely suppressed bone turnover (SSBT) patients, osteoporotic patients, and normal subjects. Bone 49, 1279–1289. https://doi.org/10.1016/j.bone.2011.09.042.

Toledano, M., Toledano-Osorio, M., Guerado, E., Caso, E., Aguilera, F.S., Osorio, R., 2018. Biochemical assessment of nanostructures in human trabecular bone: proposal of a Raman microspectroscopy based measurements protocol. Injury 49, S11–S21. https://doi.org/10.1016/j.injury.2018.07.034.

Vale, A.C., Pereira, M.F.C., Maurício, A., Amaral, P., Rosa, L.G., Lopes, A., Rodrigues, A., Caetano-Lopes, J., Vidal, B., Monteiro, J., Fonseca, J.E., Canhão, H., Vaz, M.F., 2013. Micro-computed tomography and compressive characterization of trabecular bone. Colloids Surfaces A Physicochem. Eng. Asp. 438, 199–205. https://doi.org/10.1016/j.colsurfa.2013.01.057.

Vesper, E.O., Hammond, M.A., Allen, M.R., Wallace, J.M., 2017. Even with rehydration, preservation in ethanol influences the mechanical properties of bone and how bone responds to experimental manipulation. Bone 97, 49–53. https://doi.org/10.1016/j.bone.2017.01.001.

Zhang, Z.M., Li, Z.C., Jiang, L.S., Jiang, S.D., Dai, L.Y., 2010. Micro-CT and mechanical evaluation of subchondral trabecular bone structure between postmenopausal women with osteoarthritis and osteoporosis. Osteoporos. Int. 21, 1383–1390. https://doi.org/10.1007/s00198-009-1071-2.

Zysset, P.K., Guo, X.E., Hoffler, C.E., Moore, E.K., Goldstein, S.A., 1999. Elastic modulus and hardness of cortical and trabecular bone lamellae measured by nanoindentation in the human femur. J. Biomech. 32, 1005–1012. https://doi.org/10.1016/S0021-9290(99)00111-6.